2020 IEEE International Conference on Robotics and Automation (ICRA)
31 May - 31 August, 2020. Paris, France

Adaptive Authority Allocation in Shared Control of Robots Using Bayesian Filters

Ribin Balachandran[1], Hrishik Mishra[1], Matteo Cappelli[1], Bernhard Weber[1], Cristian Secchi[2], Christian Ott[1] and Alin Albu-Schaeffer[1,3]

***Abstract*— In the present paper, we propose a novel system-driven adaptive shared control framework in which the autonomous system allocates the authority among the human operator and itself. Authority allocation is based on a metric derived from a Bayesian filter, which is being adapted online according to real measurements. In this way, time-varying measurement noise characteristics are incorporated. We present the stability proof for the proposed shared control architecture with adaptive authority allocation, which includes time delay in the communication channel between the operator and the robot. Furthermore, the proposed method is validated through experiments and a user-study evaluation. The obtained results indicate significant improvements in task execution compared with pure teleoperation.**

***Index Terms*— Adaptive authority allocation, shared control, teleoperation, Kalman filter, Bayesian filters**

I. Introduction

Autonomous robots highly rely on environment perception, which could get degraded by various internal and external factors. In particular, concerning vision-based systems, the internal factors include, among others, noise and its time-varying nature, and communication failures. In adverse cases, the perception of the robot may be negatively affected because of occlusions/image-losses caused by its own motion, as typified in Fig. 1. Control problems that address tracking and handling target objects using eye-in-hand cameras are affected by close range vision degradation or the target going out of the image [1]. Concerning external factors, sensing capabilities in field robotics may be affected by illumination changes, reflections, and shadows on the tracked object [2].

Although automatic control systems (ACS) applied to autonomous robots have been demonstrated to be capable of implementing sensitive and complicated tasks [3]–[5], a human supervision in the control loop is preferable to appropriately address unforeseen changes in the environment or robot behavior (see [6, T. 8.1]). Combining these two concepts leads to a broad control paradigm referred to as shared control [7]–[11]. One of the methods defined in this paradigm is *mixed-initiative*, in which the control commands to the robot are shared between an ACS and a human operator using teleoperation [12], [13]. The weights for sharing the control authority are called authority allocation (AA) factors [14]. Robotic task-space based load sharing of authority has been investigated in [15]–[19]. Fixed AA gains have been employed in [20]–[22] and have been made flexible by using variable or adaptive authority allocation (AAA) methods as described in [6], [23]–[25]. Adaptation methods can be based on human intention recognition [26], [27] and probabilistic approaches [28], [29]. The aforementioned list of research in shared control is not and cannot be exhaustive.

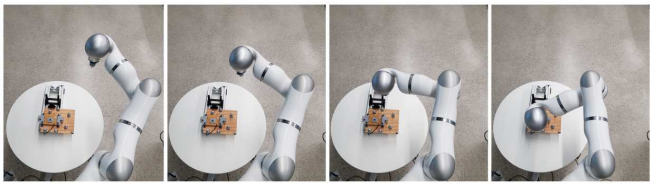

Fig. 1: Example of a high precision industrial task during which the camera view is occluded by the robotic arm itself (right-most).

The present paper is focused on a particular way of adaptation called system-driven adaptation in which the system resolves authority allocation between the two control agents and its timing [30]. In [31], related to the method proposed in the present paper, the trajectory commanded to the robot is a weighted sum of the trajectories generated by the ACS and commanded by the human. AA is based on the uncertainty of the autonomous controller using an *a priori* noise model. This might result in modeling errors in the case of time-varying noise characteristics and the robot will not react to the changes in the real environment adequately. To the best of our knowledge, there has been no research work presented to address system-driven adaptation that depends on real measurements and aimed to cope with delays in teleoperation while ensuring stability of the shared control architecture. The main contributions of the present paper are as follows:

1) We propose a novel metric based on an adaptive Bayesian filtering framework that facilitates AAA depending on sensor measurements.
2) We ensure the stability of the proposed time-delayed shared control system by exploiting the time domain passivity approach (TDPA) [32].
3) We perform experimental validation and a user-study to evaluate the usability of the proposed system-driven adaptation method.

To this end, firstly we introduce the ACS as a passivity-based Cartesian proportional-derivative (PD) controller in Sec. II and highlight the problem of noisy measurements. In Sec. III, significance of adaptive Bayesian filtering for time-varying noise uncertainty is outlined. The main contributions

[1]The department for Analysis and Control of Advanced Robotic Systems, German Aerospace Center (DLR), Germany ribin.balachandran@dlr.de
[2]University of Modena and Reggio Emilia, Modena, Italy
[3]The Faculty of Informatics, Technical University of Munich, Germany

are presented in Sec. IV, in which, we firstly propose the enhancement of the conventional 4-channel architecture bilateral controller [33] (which is made passive using TDPA as in [34], [35]), with vision-based autonomy. Secondly, we propose a metric based on the adaptive Bayesian filtering framework to enable AAA by using real measurements, which is followed by a detailed stability analysis. To validate the usability of the proposed system, in Sec. V, we summarize the results of the conducted experiments and a user-study, and present the performance comparison with pure teleoperation. In the user-study, the participants were required to complete two tasks: one notably being universal serial bus (USB) plug insertion, which required high accuracy in both, positioning and force application. Finally, we discuss the concluding remarks and possible future directions in Sec. VI.

II. Automatic Control System (ACS)

The task of the ACS is to regulate the end-effector pose, $g_s \equiv \{p_s, \theta_s\}$, about a Cartesian setpoint $g \equiv \{p, \theta\}$ as shown in Fig. 2, where $g_s, g \in SE(3)$. To this end, the ACS in the present paper is implemented as a passivity-based Cartesian PD controller on a n-joint (revolute) non-redundant slave robot. For this robot, the end-effector pose, $g_s(q) : \mathbb{R}^n \rightarrow SE(3)$, is a objective forward kinematics map of its joint configuration $q \in \mathbb{R}^n$, whose differential is written as, $\mathrm{V}_s = J(q)\dot{q} \in \mathbb{R}^6$, where V_s is the end-effector body velocity and $J(q)$ is the corresponding Jacobian map. Using this Jacobian transformation, the Cartesian dynamics can be written as,

$$\Lambda(q)\dot{\mathrm{V}}_s + \mu(q, \mathrm{V}_s)\mathrm{V}_s + \Gamma(q) = \mathrm{F}_a, \tag{1}$$

where $\Lambda(q)$, $\mu(q, \mathrm{V}_s)$, $\Gamma(q)$ and F_a refer to the matrices of Cartesian inertia and Coriolis/centrifugal terms, gravity terms, and Cartesian control forces, respectively, and joint torques are given as, $\tau = J(q)^T \mathrm{F}_a$ (see [36, §5.4]).

Lemma 1: For an n-joint (revolute) non-redundant robot whose Cartesian dynamics are defined by (1), for a desired setpoint $g \equiv (p, q)$ (see Fig. 2), the control law,

$$\mathrm{F}_a = -\gamma(\mathrm{K}_p, g, g_s) - D\mathrm{V}_s, \text{ (see } F_{PD} \text{ in [37, Th. 6])}, \tag{2}$$

ensures uniform asymptotic stability of error dynamics, where K_p and D are diagonal and positive matrices for Cartesian stiffness and damping, respectively, and $\gamma(\mathrm{K}_p, g, g_s) = d\phi(\mathrm{K}_p, g, g_s)$ (denoted by orange in Fig. 2) is the differential of a potential function on the Cartesian error that drives (1) towards the setpoint g.

Proof: For the considered regulation case, the additional tracking terms in [Th. 6] [37] can be omitted. Therefore, for the dynamics system (1), the controller in (2) ensures uniform asymptotic stability. ■

For a vision-based feedback system which provides a noisy measure of g as $\tilde{g} \equiv (\tilde{p}, \tilde{\theta})$, which is dashed in Fig. 2 and is formally modeled later in Sec. III, the control law in Lemma 1, is written as, $\mathrm{F}_a = -\gamma(\mathrm{K}_p, \tilde{g}, g_s) - D\mathrm{V}_s$. This shows that the stiffness term gets affected by the degraded measurements and hence makes the ACS vulnerable to it. In the rest of the paper, the following definition is used.

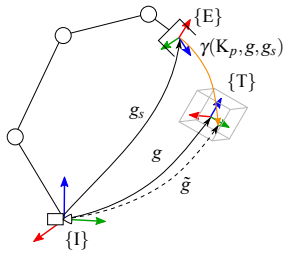

Fig. 2: Diagrammatic description of the task in which an inertial vision-based measurement, $\tilde{g} \equiv \{\tilde{p}, \tilde{\theta}\}$ (dashed), is used to regulate the inertial end-effector pose, $g_s \equiv \{p_s, \theta_s\}$, about the inertial setpoint $g \equiv \{p, \theta\}$.

Def. 1: Given $\alpha, \beta \in [0, 1]$, $\alpha(t) + \beta(t) = 1$, the authority allocation blending function [12] is, $\mathrm{F}_s = \alpha(t)\mathrm{F}_t + \beta(t)\mathrm{F}_a$, where F_a, F_t and F_s are the ACS force, teleoperation force and the total commanded force to the slave respectively.

The main objective of the present paper is to scale F_a with gain β (see Def. 1) when measurement degradation occurs. As Bayesian filters provide an associated uncertainty of the measurements, in Sec. IV-A, this uncertainty is related to β (or α) to achieve the objective.

III. Uncertainty in ACS

In this section, the dynamic model for a static setpoint frame {T} (see Fig. 2) is provided and the significance of an adaptive Bayesian filter [38, ch. 2] is outlined. For the sake of completeness, we first describe a simple zero-acceleration stochastic process model for {T}, whose state is, $x = \begin{bmatrix} p^T & v^T & \theta^T & \omega^T \end{bmatrix}^T \in \mathbb{R}^3 \times \mathbb{R}^3 \times \mathbb{Q} \times \mathbb{R}^3$, where $\mathbb{Q} \equiv \{\theta \in \mathbb{R}^4 | \ ||\theta|| = 1\}$ is the quaternion manifold. The dynamic model and the output function are written as,

$$\dot{x} = f(x), \ y = h(x), \ f(x) = \begin{bmatrix} v \\ v_v \\ \frac{1}{2}\omega \otimes \theta \\ v_\omega \end{bmatrix}, \ h(x) = \begin{bmatrix} \tilde{p} \\ \tilde{\theta} \end{bmatrix}, \tag{3}$$

where $g \equiv \{p, \theta\} \in \mathbb{R}^3 \times \mathbb{Q} \equiv SE(3)$ denotes the pose of {T} relative to {I}, which is a part of the state x and is measured in this case (see Fig. 2), the velocities v and ω are the inertial linear and body angular velocities respectively, and $\otimes$ is the quaternion multiplication operator. The process noise in (3) is $v = \begin{bmatrix} v_v^T & v_\omega^T \end{bmatrix}^T \in \mathbb{R}^6$ and $Q = \mathbb{E}(vv^T)$ is the process covariance, where $\mathbb{E}(\bullet)$ is the stochastic expectation of the argument. The measurement noise model is $\tilde{p} = p + \mu_p$ and $\tilde{\theta} = \begin{bmatrix} \mu_\theta \\ 1 \end{bmatrix} \otimes \theta$, $\mu = \begin{bmatrix} \mu_p^T & \mu_\theta^T \end{bmatrix}^T \in \mathbb{R}^6$, with measurement noise covariance $R = \mathbb{E}(\mu\mu^T)$. For Bayesian filtering, (3) is used as the stochastic model to provide a filtered pose $\hat{g} \equiv \{\hat{p}, \hat{\theta}\}$ corresponding to the state g. A full quaternion representation of θ is not admissible in the Bayesian filtering framework due to the unity constraint and results in covariance degeneracy [39]. As a result, an unconstrained 3-parameter $a \in \mathbb{R}^3$ is used for the quaternion representation such that $\mathbb{E}(a) = 0_{3,1}$. So, simply by replacing θ with a, we obtain a modified state $X = \begin{bmatrix} p^T & v^T & a^T & \omega^T \end{bmatrix}^T$, using which we obtain a state error $\delta X = (X - \hat{X})$, whose state

covariance is given by $P = \mathbb{E}\big(X(x)X(x)^T\big)$. In Bayesian filtering, P is the covariance of the state x in (3).

In the classical Bayesian pose estimation problem, *a priori* knowledge of uncertainties in measurement noise (R) and model (Q) is assumed and if the assumption holds, the automatic controller is fully capable of performing the task by simply using a filtered pose $\hat{g}$. However, in some practical cases, while the physical model uncertainty (Q) is well known, the measurement uncertainty (R) for a vision-based system, especially in cases of occlusion and high contrast, is time-varying. This means that there is a time-varying uncertainty in the setpoint pose (g) about which the ACS regulates. This negatively affects $\hat{g}$ and will cause ACS errors as pointed out in Sec. II. Using $\hat{g}$ in (2) results in an interconnection of a Bayesian filter and ACS, and for the sake of ease of illustration of passivity of the proposed method, in this paper, $\tilde{g}$ is used in (2). If the passivity of the aforementioned interconnection can be established, the proposed method can also use $\hat{g}$ in (2); however, this is not in the scope of the present paper.

In the common class of Bayesian filters, for example, in the extended Kalman filter (EKF), the time-evolution of P is independent of real measurements and hence the change in state uncertainty due to such a measurement degradation is not reflected. To address this issue, we use adaptive filtering techniques [40]–[42], which use measurement data ($\tilde{g}$) to estimate the measurement noise uncertainty (R). Note that in the Bayesian filtering framework, the state covariance $P(t)$ also gets adapted due to its dependence on the adapted measurement uncertainty $R(t)$.

IV. Proposed Method

In this section, for the time-varying covariance (P) of the setpoint g, firstly, a mapping to the AAA factor α (see Def. 1) is proposed. Secondly all the constituents are merged to formulate the proposed shared control framework. Thirdly, stability of the shared control framework is established.

A. Proposed Mapping between $\alpha(t)$ and $P(t)$

An adaptive Bayesian filter is with the purpose to map its uncertainty measure to the time-varying gain, β, to scale down the ACS forces (in the case of measurement degradation) and to transfer authority to the human operator who completes the task due to increase in α, see Def. 1. To this end, the authority of the human operator α, which was defined earlier in Sec. IV, is derived from the time-varying covariance $P(t)$ of the adaptive Bayesian filter as:

$$\alpha(t) = \begin{cases} \frac{\xi\left(P(t)\right)-\xi(\underline{P})}{\xi(\overline{P})-\xi(\underline{P})} & \text{if } \xi(\underline{P}) \leq \xi\left(P(t)\right) \leq \xi(\overline{P}) \\ 0 & \text{if } \xi\left(P(t)\right) < \xi(\underline{P}) \\ 1 & \text{if } \xi\left(P(t)\right) > \xi(\overline{P}), \end{cases} \tag{4}$$

where $\xi(\bullet) = \log\big(\text{trace}(\bullet)\big)$. $\underline{P}$ and $\overline{P}$ correspond to the state covariance matrices for good and consistently degraded measurements respectively, which are *a priori* identified for the estimation system in hand as follows. Before beginning the task execution, the adaptive Bayesian filter is allowed to converge, which provides a reliable estimate of $\underline{P}$, whereas an upper bound $\overline{P}$ is obtained by performing the task using ACS and noting $P(t)$ when it fails due to consistently degraded measurements.

In summary, when ACS gets degraded measurements, the value of α increases and the authority is accordingly shifted to the human operator. This can be clearly seen in the experiment plots shown in Fig. 6.

As an example, we demonstrate adaptation of R in a common Bayesian filter, namely, EKF [43] for the system defined in (3), which is used for experimental validation in Sec. V. The design adopted from [44], which modeled a moving $\{\text{T}\}$ therein, can trivially be modified for a static $\{\text{T}\}$ by using (3) (zero acceleration). In [44, §4.A], the time-varying nature of R for vision-based systems was highlighted and addressed using a a residual-based recursive adaptation technique. In the present paper, however, the adaptation is performed using a similar method as in [42] that resembles *covariance matching* [40] for the k^{th} step as follows:

$$R_k = \eta\, R_{k-1} + (1-\eta)\,(\varepsilon_k\, \varepsilon_k^T + H_k\, P_k^-\, H_k^T),$$

where $\eta \in (0,1)$ is a forgetting factor and $\varepsilon \in \mathbb{R}^6$ is the measurement residual obtained after the measurement update. *We outline, that by adapting $R(t)$ online in this way, the state covariance matrix $P(t)$, which depends on $R(t)$, gives a reliable uncertainty metric of the regulation state g.* In the present paper, without any loss of generality, we use the *covariance matching* adaptive EKF for state estimation for experimental evaluation, although any of the other methods, including a particle filter [38, ch. 7], may be employed as well.

B. Proposed Shared Control Architecture

For the teleoperation part of the proposed shared control framework (see one-DoF representation in Fig. 3), the conventional 4-channel architecture bilateral controller [33] is used where the positions (V_m, V_s) and measured forces (F_h, F_e) are exchanged between the master and slave devices. This approach is represented in the signal flow diagram provided in Fig. 3 in black. The variables $(\bullet)'$ are the delayed variants of the argument arising due to communication delays (T_f from master to slave and T_b backward). F_{cm} and F_{cs} are the forces produced by the position controllers locally at the master and slave respectively. C_1, C_2 and C_3 are the gains for the forces from the local master controller, human and the environment respectively. The teleoperation system is ensured to be passive using TDPA according to [34]. For the sake of brevity, the details of the passivation techniques are omitted and can be found in [34].

The contribution (denoted in blue and red in Fig. 3)) of the present paper is the enhancement of the aforementioned teleoperation system by adding the ACS which is based on visual tracking to form the shared control system. V_T is the velocity of the target $\{\text{T}\}$ commanded to ACS (0 in this case). P refers to the state covariance defined in Sec. III and α, β are defined in Def. 1. As can be seen, the commanded

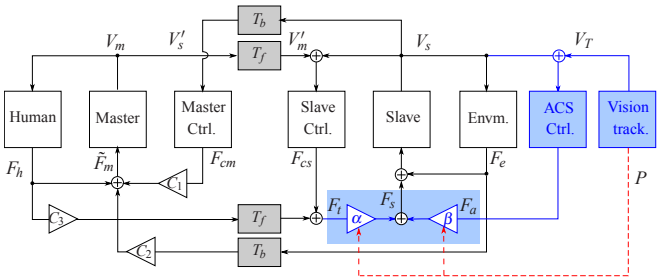

Fig. 3: Signal-flow diagram of the proposed shared control framework.

force to the slave, F_s, is the weighted sum of teleoperation force F_t and ACS force F_a (according to Def. 1).

C. Stability Analysis

The overall shared control system presented in Fig. 3 can be considered as an interconnection of subsystems, for which the one-DoF port representation is provided in Fig. 4. In this section, the stability of the proposed multi-DoF shared control system with AAA is analysed. Firstly, from Lemma 1, if $\beta = 1$, the ACS is uniformly asymptotically stable, and is passive with $(\mathrm{F}_a, \mathrm{V}_s)$ as power-correlated variables [45]. When $\beta = 0$, the authority is completely allocated the human operator and the system behaves as a pure teleoperation controller. As explained in Sec. IV, we use a 4-channel architecture for the bilateral controller which has been made passive by using the same TDPA approach as in [34], [35]. For $0 < \alpha, \beta < 1$, the passivity of the system is analyzed based on the 3-port network represented in Fig. 4. The human, slave robot and the ACS interact with the system through the power ports $P_1 : (\mathrm{F}_m, \mathrm{V}_m)$, $P_2 : (\mathrm{F}_s, \mathrm{V}_s)$ and $P_3 : (\mathrm{F}_a, \mathrm{V}_s)$, respectively. It should be noted that $(\mathrm{F}_i, \mathrm{V}_i)$ are the multi-DoF representation of the one-DoF analog provided in Fig. 4. The passivity of the 3-port network is maintained by ensuring that the energy flowing out of the system is never greater than the energy flowing in (see Fig. 4), that is, $\sum_{i=1}^{3}(E_i^{in} - E_i^{out}) \geq 0$. This is equivalent to:

$$\int_0^t (\mathrm{F}_m^T \mathrm{V}_m + \mathrm{F}_a^T \mathrm{V}_s + \mathrm{F}_s^T \mathrm{V}_s) dt \geq 0. \tag{5}$$

This is the passivity condition for a 3-port network in a system with zero initial energy [32]. By designing a passivity observer (PO) and passivity controller (PC) for each port, as described in [32], we can ensure the passivity of the 3-port network. In the proposed system, $E_{obs,i}$ is the observed

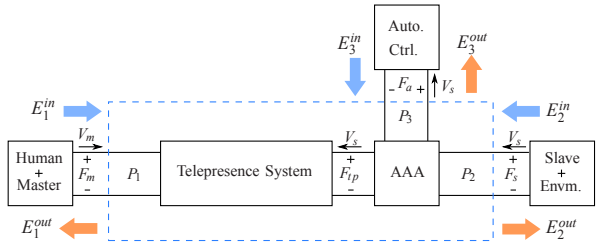

Fig. 4: Port representation of the proposed shared control system with energy flows.

energy flow in port P_i after applying the PC and is defined as:

$$\begin{aligned} E_{obs,i}(k) = E_{obs,i}(k-1) + \mathrm{F}_i(k)^T \mathrm{V}_i(k) T \\ + \mathrm{F}_{pc,i}(k-1)^T \mathrm{V}_{pc,i}(k-1) T, \end{aligned} \tag{6}$$

where i iterates over the 3 ports, and F_i and V_i are the force and velocity of the port P_i respectively, corresponding to the three terms in (5). Note that in contrast to the integral form provided in (5), an analogous discrete representation in (6) has been used assuming a fast sampling time T. The terms $\mathrm{F}_{pc,i}$ and $\mathrm{V}_{pc,i}$ are described now. PC is a time-varying damper added to the system if the PO observes any activity in the port ($E_{obs,i} < 0$). In the 3-port network here, the total observed energy is $E_{obs}^{tot} = \sum_{i=1}^{3} E_{obs,i}$. PC can be applied both in impedance causality (modifies force if it is the port output) and in admittance causality (modifies velocity if it is the port output). In the 3-port network presented in Fig. 4, the output of the two ports is force (P_1, P_2), whereas that of the ACS port (P_3) is the slave velocity. For the force output ports, the PC is a damping element $R_{pc,i} \quad i \in [1,2]$ defined as follows:

$$R_{pc,i}(k) = \begin{cases} -\frac{E_{obs}^{tot}(k)}{\mathrm{V}_i(k)^T \mathrm{V}_i(k) T} & \text{if } E_{obs}^{tot}(k) < 0 \\ 0 & \text{else.} \end{cases} \tag{7}$$

The force $\mathrm{F}_{pc,i}$ and velocity $\mathrm{V}_{pc,i}$ in (6) are given by:

$$\mathrm{F}_{pc,i}(k) = R_{pc,i}(k) \mathrm{V}_i(k), \quad \mathrm{V}_{pc,i}(k) = \mathrm{V}_i(k). \tag{8}$$

For the port P_3 where the output is velocity V_s, a PC with admittance causality is used and the output velocity is modified. Here, the damping element $R_{pc,3}$ is formulated as:

$$\frac{1}{R_{pc,3}(k)} = \begin{cases} -\frac{E_{obs}^{tot}(k)}{\mathrm{F}_a(k)^T \mathrm{F}_a(k) T} & \text{if } E_{obs}^{tot}(k) < 0 \\ 0 & \text{else.} \end{cases} \tag{9}$$

The force $\mathrm{F}_{pc,3}$ and velocity $\mathrm{V}_{pc,3}$ in (6) are given by:

$$\mathrm{F}_{pc,3}(k) = \mathrm{F}_a(k), \quad \mathrm{V}_{pc,3}(k) = \mathrm{F}_a(k) / R_{pc,3}(k). \tag{10}$$

The 3-port network with the *PC*s on all ports are shown in Fig. 5. F_m', F_s' and V_s' are the modified forces and velocity of the three ports respectively. It has to be noted that in the present work, the activity removed by one *PC* has not been considered while computing the damping terms for the other two ports, which will be addressed in future work. In this way, the 3-port network of the shared control scheme is made passive. The Slave + Envm port is passive, the ACS port was proven to be passive [45], and it is widely accepted that the human and master (although being a source of energy in the system) is passive. The system represented in Fig. 5, is thus an interconnection of passive systems and is thus stable [46, Th. 6.3]

V. Experiments and User-Study

A shared control station was set up to validate the feasibility of the proposed method. A KUKA light-weight-robot (LWR) master and an LWR slave were employed to complete two tasks. The first task T_1 was to insert the USB male port (fixed on the slave end-effector) into a USB female port that

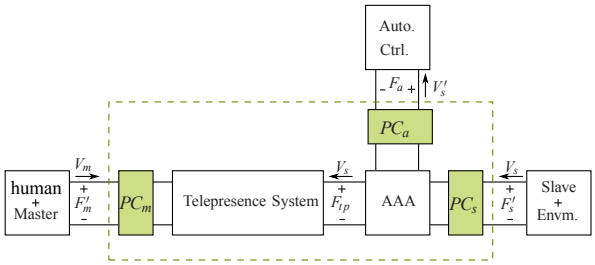

Fig. 5: Port representation of the proposed shared control system with passivity controllers.

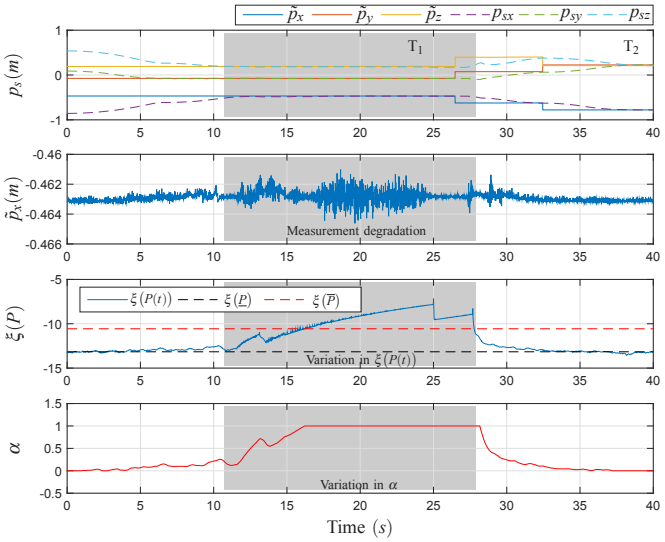

Fig. 6: Variation in α with variation in measurement noise

was fixed on the work table. Once T_1 was complete (which was signaled by a green LED bulb on the work-object), the male USB port had to be ejected. The second task T_2 was to move to the other end of the work table and to insert the same USB male port at the slave end-effector into the set-up with a larger insertion point (to simulate a tool changer). Both tasks, T_1 and T_2, were executed sequentially with pure teleoperation (TO) and also with the proposed shared control (SC). In both cases, a round trip delay of 200ms was simulated between the master and the slave. The operator station was composed of the master, a monitor with webcam views of the work environment of the slave, a graphical user interface (GUI) to visualize the current AA factor α. To further assist the operator, a vibro-tactile feedback was provided whenever the authority (α) crossed the 0.5 value. In SC, the pose of the USB female port ($\{T\}$) was tracked by a vision-based tracker. The ACS moved the slave robot from its initial position to T_1 target point and the master device also followed the slave (due to the position coupling of the 4-channel bilateral controller). As the slave end-effector approached T_1 target point, the view on the tracked target was occluded by the slave robot itself (see Fig. 1). This led to the deterioration of measurements from the tracking system, and resulted in a shift in authority from ACS to the human operator due to the increase in α, as explained in Sec. III. The human operator completed the final operation of inserting the USB male port and then moved towards T_2 target point. As soon as the slave robot moved away and the occlusion was removed, the vision-based tracker started providing good measurements and the covariance of the adaptive EKF reduced and consequently, α. As a result, the ACS regained control and helped the human operator approach T_2 target point.

In Fig. 6, the top plot represents the desired $\tilde{p} = \begin{bmatrix}\tilde{p}_x & \tilde{p}_y & \tilde{p}_z\end{bmatrix}^T$ and actual values $p_s = \begin{bmatrix}p_{sx} & p_{sy} & p_{sz}\end{bmatrix}^T$ of the slave tool center point, which shows agreement between the two, and demonstrates convergence of SC. The second plot shows the position of the target measured by the vision-based tracker. For clarity, *only* $\tilde{p}_x$ *is shown*, which highlights the measurement degradation between $11s - 27s$ The third plot shows the variation in $\xi\left(P(t)\right)$ with measurement degradation in the same period, which demonstrates the effectiveness of the adaptive EKF. The fourth plot shows the consequent variation of α (see (4)) . It can be seen that when the measurements are degraded, α increases and when the measurements are good after (T_1), α decreases. This validates the adaptive SC approach proposed in the paper. The records of the tasks being executed, in both pure TO mode and SC mode are presented in the accompanying video submission.

A. User study analysis

To verify whether the proposed shared control approach really assists a human operator in executing tasks that require high precision (USB insertion), a user study was conducted. Below, we present the details of the study:

1) Method: T testing sample N = 14 male employees of DLR with an average age of 27.93 years (SD= 5.6 years, Range: 22-43 years) participated in the present study after having signed an informed consent form.

2) Experimental Task: All the participants had to complete T1, and then T2 as mentioned in Sec. V.

3) Experimental Design: A within-subject design was applied, namely, each subject completed both TO and SC modes subsequently, with the order of modes counterbalanced across the participants. There were two trials with both modes, resulting in two experimental schemes: 1. TO-SC-TO-SC; 2. SC-TO-SC-TO.

4) Procedure: After having completed a demographic questionnaire, the subjects were briefly introduced into the concepts of TO and SC. The tasks described in Sec. V were explained to them and a training with duration of 5 minutes was conducted to complete the tasks both in the TO and SC modes. After the training, the actual experimental trials started. After completing an experimental tasks, subjects were administered a brief questionnaire with one item measuring the overall workload ("Please rate your overall workload during the last task", adapted from the OWS scale [47], and one item measuring physical demands ("How physically demanding was the last task", adapted from the NASA-TLX scale [48]. Both items were rated on a 20-point bipolar scale ranging from "very low" to "very high". After

having finished the entire experiment, a final questionnaire with several items on situation awareness during the SC mode was filled out by participants (in the 8-point Likert-like response format ranging from "does not apply at all" to "completely applies").

5) Data Analysis: The repeated measure analysis of variance (rmANOVA) with Conditions (TO vs. SC) and Trial (1 vs. 2) as within factors was conducted on completion time, mean forces, mean torques, the workload as well as physical demand ratings. Descriptive data (mean M and standard deviation SD) were calculated for the ratings in the final query.

6) Results: Based on the objective and subjective data analyzed during the study, the following results were obtained:

Completion time: RmANOVA revealed a non-significant trend for Condition $(F(1,13) = 2.9,\ p = 0.11)$, namely, completion times tended to be shorter with SC (M = 64.4s) compared with TO (M = 77.3s). Furthermore, Trial reached significance $(F(1,13) = 11.1,\ p < 0.01)$, indicating a learning effect from trials 1 to 2.

Mean forces and torques: Regarding mean forces, neither Control $(F(1,13) = 0.03)$ nor Trial $(F(1,13) = 0.14)$ reached significance. Yet, a significant Control main effect was found in rmANOVA on mean torques $(F(1,13) = 10.7,\ p < .01)$, i.e. the average torques were significantly lower with SC (M= 0.059) compared to TO (M = 0.072).

Subjective Ratings: RmANOVA yielded a significant Control $(F(1,13) = 11.6,\ p < 0.01)$ and Trial main effect $(F(1,13) = 6.57,\ p < 0.05)$ on overall workload ratings. Subjects' rating were significantly higher during TO (M= 9.43) compared with SC (M = 5.32) and the workload was indicated to be lower in the 2. trial (trial 1: 8.25, trial 2: 6.50). Regarding physical demand, only a Control main effect was evident $(F(1,13) = 12.1,\ p < 0.01)$, with significantly lower ratings for SC (M = 4.96; TO: M= 9.04).

Situational awareness: Ratings of the final questionnaire on situation awareness (SA) during SC indicated that subjects mainly felt to be aware of the positions and actions of the robots (M = 6.43; SD =1.16), felt capable of anticipating robot's actions (M =6.0; SD =1.75), and were mainly aware of the degree of control they had (M =6.29; SD =1.94). Moreover, they rated the vibro-tactile feedback as being helpful to maintain SA (M =6.36; SD =2.13). Only the ratings whether the GUI was helpful with regard to SA reached rather moderate approval (M =4.64; SD =1.99).

B. Discussion

The insertion of the USB port using TO with delay is a task that requires high accuracy in both position, orientation and force application. The objective evaluation indicates that the physical effort has been reduced while implementing the task in the SC mode. The improvement has been mainly achieved in terms of the amount of torque input (18% reduction with SC) from the operator since the ACS already places the end-effector USB port in the right orientation before the human operator gets control. He needs to complete only the final insertion, which is not the case in pure teleoperation where he has to execute the task from beginning. The subjective evaluation shows significant reduction in the physical (45.13%) and overall workload (43.58%) of the participants during the task execution. This can be explained by the fact that in SC mode the participant was relieved of most of the work and had to intervene only when the autonomous system could not complete the task. Overall, despite the short training time, the results indicate a reduction in the completion time (16.7%), torque input from the participant and workload, both physical and overall, with the SC approach.

Lessons learned: In terms of situational awareness, the user study indicates that the multi-modal feedback provided to the participants (kinesthetic and vibro-tactile feedback from the master device and the visual feedback of the slave environment and α value in the GUI) was overall helpful for the participants. However, 2 out of the 14 participants reported that the amount of information was excessive, which increased their cognitive load (specifically, monitoring the GUI while observing the webcam views and inserting the USB plugs). A better method, possibly a head mounted display which gives a single, 3D view of the work environment and that is augmented with the α value, has to be developed.

Although it was generally reported by the participants and was verified in the subjective and objective analysis that the SC scheme reduced the overall workload of the operators, 3 out of 14 participants mentioned that an option for human intervention was missing and they could not override the ACS commanded slave motion. This can be seen as a limitation of the proposed system-driven adaptation method.

VI. Conclusion

In the present paper, a shared control system with adaptive authority allocation was proposed. Unlike in the previous related works, the AA mechanism proposed in this paper was not fixed *a priori*. The adaptation was established based on a metric derived from an adaptive EKF's state covariance which depended on the real sensor measurements. This allowed the ACS to execute the tasks and yield control authority to the operator only when the measurements degraded. A subjective evaluation based on a user-study indicated the benefits of the proposed approach, which relieved the operator of significant amount of workload. It has to be noted that in this work, only the occlusion scenario for Vicon trackers was presented to introduce the concept. This method can be applied in other tracking systems like cameras and lidars, and can be used to address other practical issues like camera noise (due to close-range and large-angle targets), image losses and changes in lighting conditions (shadows, specularities etc). The application of the proposed method to these scenarios will be investigated in future research work. Other future research plans include extending the work to moving targets, enabling human intervention and optimizing the passivity criteria for better performance.

REFERENCES

[1] D. A. Forsyth and J. Ponce, *Computer vision: a modern approach*. Prentice Hall Professional Technical Reference, 2002.

[2] P. W. Schmidt, R. Balachandran, and J. A. Esclusa, "Shared control for robotic on-orbit servicing," 2016.

[3] K. Nottensteiner, M. Sagardia, A. Stemmer, and C. Borst, "Narrow passage sampling in the observation of robotic assembly tasks," in *2016 IEEE International Conference on Robotics and Automation (ICRA)*. IEEE, 2016, pp. 130–137.

[4] S. Thrun *et al.*, "Robotic mapping: A survey," *Exploring artificial intelligence in the new millennium*, vol. 1, no. 1-35, p. 1, 2002.

[5] J. De Schutter, T. De Laet, J. Rutgeerts, W. Decré, R. Smits, E. Aertbeliën, K. Claes, and H. Bruyninckx, "Constraint-based task specification and estimation for sensor-based robot systems in the presence of geometric uncertainty," *The International Journal of Robotics Research*, vol. 26, no. 5, pp. 433–455, 2007.

[6] T. Inagaki *et al.*, "Adaptive automation: Sharing and trading of control," *Handbook of cognitive task design*, vol. 8, pp. 147–169, 2003.

[7] S. Hayati and S. Venkataraman, "Design and implementation of a robot control system with traded and shared control capability," in *Proceedings, 1989 International Conference on Robotics and Automation*. IEEE, 1989, pp. 1310–1315.

[8] T. B. Sheridan, "Telerobotics," *Automatica*, vol. 25, no. 4, pp. 487–507, 1989.

[9] T. B. Sheridan, *Telerobotics, automation, and human supervisory control*. MIT press, 1992.

[10] A. Franchi, C. Secchi, M. Ryll, H. H. Bulthoff, and P. R. Giordano, "Shared control: Balancing autonomy and human assistance with a group of quadrotor uavs," *IEEE Robotics & Automation Magazine*, vol. 19, no. 3, pp. 57–68, 2012.

[11] D. A. Abbink, M. Mulder, and E. R. Boer, "Haptic shared control: smoothly shifting control authority?" *Cognition, Technology & Work*, vol. 14, no. 1, pp. 19–28, 2012.

[12] S. Musić and S. Hirche, "Control sharing in human-robot team interaction," *Annual Reviews in Control*, vol. 44, pp. 342–354, 2017.

[13] H. Saeidi, F. McLane, B. Sadrfaidpour, E. Sand, S. Fu, J. Rodriguez, J. R. Wagner, and Y. Wang, "Trust-based mixed-initiative teleoperation of mobile robots," in *2016 American Control Conference (ACC)*. IEEE, 2016, pp. 6177–6182.

[14] R. Parasuraman and V. Riley, "Humans and automation: Use, misuse, disuse, abuse," *Human factors*, vol. 39, no. 2, pp. 230–253, 1997.

[15] F. Abi-Farraj, N. Pedemonte, and P. R. Giordano, "A visual-based shared control architecture for remote telemanipulation," in *2016 IEEE/RSJ International Conference on Intelligent Robots and Systems (IROS)*. IEEE, 2016, pp. 4266–4273.

[16] H. Boessenkool, D. A. Abbink, C. J. Heemskerk, F. C. van der Helm, and J. G. Wildenbeest, "A task-specific analysis of the benefit of haptic shared control during telemanipulation," *IEEE Transactions on Haptics*, vol. 6, no. 1, pp. 2–12, 2012.

[17] M. Lawitzky, A. Mörtl, and S. Hirche, "Load sharing in human-robot cooperative manipulation," in *19th International Symposium in Robot and Human Interactive Communication*. IEEE, 2010, pp. 185–191.

[18] M. Selvaggio, P. R. Giordano, F. Ficuciello, and B. Siciliano, "Passive task-prioritized shared-control teleoperation with haptic guidance," 2019.

[19] W. B. Griffin, "Shared control for dexterous telemanipulation with haptic feedback," Ph.D. dissertation, Stanford University Stanford, CA, 2003.

[20] P. Evrard and A. Kheddar, "Homotopy-based controller for physical human-robot interaction," in *RO-MAN 2009-The 18th IEEE International Symposium on Robot and Human Interactive Communication*. IEEE, 2009, pp. 1–6.

[21] M. Panzirsch, R. Balachandran, and J. Artigas, "Cartesian task allocation for cooperative, multilateral teleoperation under time delay," in *Robotics and Automation (ICRA), 2015 IEEE International Conference on*. IEEE, 2015, pp. 312–317.

[22] S. S. Nudehi, R. Mukherjee, and M. Ghodoussi, "A shared-control approach to haptic interface design for minimally invasive telesurgical training," *IEEE Transactions on Control Systems Technology*, vol. 13, no. 4, pp. 588–592, 2005.

[23] T. B. Sheridan, "Adaptive automation, level of automation, allocation authority, supervisory control, and adaptive control: distinctions and modes of adaptation," *IEEE Transactions on Systems, Man, and Cybernetics-Part A: Systems and Humans*, vol. 41, no. 4, pp. 662–667, 2011.

[24] W. B. Rouse, "Adaptive allocation of decision making responsibility between supervisor and computer," in *Monitoring behavior and supervisory control*. Springer, 1976, pp. 295–306.

[25] J. Philips, J. del R. Millan, G. Vanacker, E. Lew, F. Galan, P. W. Ferrez, H. Van Brussel, and M. Nuttin, "Adaptive shared control of a brain-actuated simulated wheelchair," in *2007 IEEE 10th International Conference on Rehabilitation Robotics*, June 2007, pp. 408–414.

[26] A. D. Dragan and S. S. Srinivasa, "A policy-blending formalism for shared control," *The International Journal of Robotics Research*, vol. 32, no. 7, pp. 790–805, 2013.

[27] A. Kucukyilmaz, T. M. Sezgin, and C. Basdogan, "Intention recognition for dynamic role exchange in haptic collaboration," *IEEE transactions on haptics*, vol. 6, no. 1, pp. 58–68, 2012.

[28] P. Trautman, "Assistive planning in complex, dynamic environments: a probabilistic approach," in *2015 IEEE International Conference on Systems, Man, and Cybernetics*. IEEE, 2015, pp. 3072–3078.

[29] R. Platt Jr, R. Tedrake, L. Kaelbling, and T. Lozano-Perez, "Belief space planning assuming maximum likelihood observations," *Proceedings of the Robotics: Science and Systems*, 2010.

[30] M. W. Scerbo, "Theoretical perspectives on adaptive automation," *Automation and human performance: Theory and applications*, pp. 37–63, 1996.

[31] P. Owan, J. Garbini, and S. Devasia, "Uncertainty-based arbitration of human-machine shared control," *arXiv preprint arXiv:1511.05996*, 2015.

[32] B. Hannaford and J.-H. Ryu, "Time-domain passivity control of haptic interfaces," *Robotics and Automation, IEEE Transactions on*, vol. 18, no. 1, pp. 1–10, 2002.

[33] D. A. Lawrence, "Stability and transparency in bilateral teleoperation," *Robotics and Automation, IEEE Transactions on*, vol. 9, no. 5, pp. 624–637, 1993.

[34] J. Rebelo and A. Schiele, "Time domain passivity controller for 4-channel time-delay bilateral teleoperation," *Haptics, IEEE Transactions on*, vol. 8, no. 1, pp. 79–89, 2015.

[35] J. Artigas, R. Balachandran, C. Riecke, M. Stelzer, B. Weber, J.-H. Ryu, and A. Albu-Schaeffer, "Kontur-2: force-feedback teleoperation from the international space station," in *2016 IEEE International Conference on Robotics and Automation (ICRA)*. IEEE, 2016.

[36] R. M. Murray, *A mathematical introduction to robotic manipulation*. CRC press, 2017.

[37] F. Bullo and R. M. Murray, "Tracking for fully actuated mechanical systems: a geometric framework," *Automatica*, vol. 35, no. 1, pp. 17–34, 1999.

[38] S. Särkkä, *Bayesian Filtering and Smoothing*. New York, NY, USA: Cambridge University Press, 2013.

[39] M. F. Lefferts E.J. and S. M.D., "Kalman Filtering for Spacecraft Attitude Estimation," vol. 5, no. 5, pp. 417–429, 1982.

[40] R. K. Mehra, "Approaches to adaptive filtering," in *1970 IEEE Symposium on Adaptive Processes (9th) Decision and Control*, Dec 1970, pp. 141–141.

[41] S. Särkkä and J. Hartikainen, "Non-linear noise adaptive kalman filtering via variational bayes," in *2013 IEEE International Workshop on Machine Learning for Signal Processing (MLSP)*, Sep. 2013.

[42] A. S. and Y. N., "Adaptive Adjustment of Noise Covariance in Kalman Filter for Dynamic State Estimation," pp. 1–5, 2017.

[43] A. Jazwinski, *Stochastic Processes and Filtering Theory*, ser. Dover Books on Electrical Engineering Series. Dover Publications, 2007. [Online]. Available: https://books.google.de/books?id=4AqL3vE2J-sC

[44] F. Aghili and K. Parsa, "Adaptive motion estimation of a tumbling satellite using laser-vision data with unknown noise characteristics," in *2007 IEEE/RSJ International Conference on Intelligent Robots and Systems*. IEEE, 2007, pp. 839–846.

[45] R. Ortega, J. A. L. Perez, P. J. Nicklasson, and H. J. Sira-Ramirez, *Passivity-based control of Euler-Lagrange systems: mechanical, electrical and electromechanical applications*. Springer Science & Business Media, 2013.

[46] H. K. Khalil, "Nonlinear systems," *Upper Saddle River*, 2002.

[47] M. A. Vidulich and P. S. Tsang, "Absolute magnitude estimation and relative judgement approaches to subjective workload assessment," in *Proceedings of the Human Factors Society Annual Meeting*, vol. 31, no. 9. SAGE Publications Sage CA: Los Angeles, CA, 1987, pp. 1057–1061.

[48] S. G. Hart and L. E. Staveland, "Development of nasa-tlx (task load index): Results of empirical and theoretical research," *Advances in psychology*, vol. 52, pp. 139–183, 1988.